SciMedCentral

Journal of Pharmacology & Clinical Toxicology

Case Report

# Photoremoval of Ethylene Vinyl Alcohol and Acrylonitrile Microplastics with S and $VO_2$ Containing Cellulose taken from Paper Industry Wastes

**Delia Teresa Sponza***

*Department of Environmental Engineering, Dokuz Eylül University, Turkey*

***Corresponding author**
Delia Teresa Sponza, Department of Environmental Engineering, Dokuz Eylül University, BUCA, İZMİR- TURKEY, Tel: 00905356932709

**Submitted:** 15 July 2024

**Accepted:** 27 August 2024

**Published:** 30 August 2024

**ISSN:** 2333-7079



**Keywords**
- Photoremoval
- Ethylene vinyl alcohol
- Acrylonitrile
- Microplastic
- S and $VO_2$ containing Cellulose
- Nanocomposite

**Abstract**

Microplastics becomes an important threat to environment and to humans due to negative impacts on health. Sunlight is known to be the natural energy source that degrades plastic waste at a very slow rate. Based on sunlight, the photocatalytic degradation process could significantly accelerate the degradation efficiency of pollutants. In this study in order to photodegrade two microplastics namely ethylene vinyl alcohol and acrylonitrile present in some paper industry wastes cellulose/S/$VO_2$ nanocomposite was generated under laboratory conditions. The effects of some operational conditions (time, ethylene vinyl alcohol and acrylonitrile concentrations, cellulose/S/$VO_2$ nanocomposite concentration) and environmental conditions (pH, temperature, sun ligth power) on the photodegradation of ethylene vinyl alcohol and acrylonitrile microplastic were investigated. For maximal photodegradation yields of ethylene vinyl alcohol (99%) and acrylonitrile (97%) microplastics the operational conditions should be as follows: 1,9 mg/l cellulose /S/ $VO_2$ nanocomposite, 700 mg/l microplastic concentration and 40 min photodegradation time. For environmental conditions the matrix should be 10, 50 oC and 60 W/$m^2$ for pH, temperature and sun ligth intensity. XRD results showed that S exhibited S8 orthorhombic structure while $VO_2$ exhibited a monoclinic structure with crystal properties. FT-IR results indicated that in the Cellulose/S-$VO_2$ nanocomposite S doped to the $VO_2$ surface. The sligthly weak band at 1709 $cm^{-1}$ on cellulose could be defined by OH groups attachements. XPS analysis results illustrated that The peak at 533.4 eV exhibits lattice O for $VO_2$ wiaximal hile maximal peak at 529.2 eV shows the C–OH and C–O–C bounds in Cellulose. The reusability studies exhibited perfect result. After 90 times utilization of the cellulose /S/$VO_2$ nanocomposite the ethylene vinyl alcohol and acrylonitrile microplastic photodegradation yields decreased sligtly to 96% and 94%, respectively

## INTRODUCTION

Microplastics have extensive types containing, pellets, films, spheres, and foams. Fiber-shaped microplastics emitted apparel industry. From the fragmentation of plastics foam plastic were produced. From packaging materials film-like structures were developed. Sphere microplastics are generated from crushing media during transportation of microplastics. The microplastics can be classified into two type according to their origins: primary microplastics and secondary microplastics. Primary microplastics, contain microbeads present in cosmetics and their diameter is < 5 mm [1,2]. These microplastics are defined as polyethylene and polypropylene. Other primary microplastics were industrial cleaning materials; plastic resin pellets and drilling materials [3,4]. Secondary microplastics are degradation products. Some countries banned the use of primary microplastics and control the production of secondary microplastics since emitted to the aquatic receiving ecosystems [5,6]. On the other hand, fragment products of the plastics originated from the erosion and as a result tiny plasticsas secondary micro- and nanoplastics were produced. Microplastics can be harmful since their diameters is small. Recent efforts to overcome and treat the plastics with conventional treatment processes did not show excellent remediation.

Ethylene vinyl alcohol (EVOH) is another ethylene copolymer, this time using the comonomer vinyl alcohol (produced by the hydrolysis of vinyl acetate). It has excellent barrier to oxygen (less than 2 cc/$m^2$/day) but the –OH groups make it hydrophilic, i.e. it attracts water, which decreases the oxygen barrier. Ethylene vinyl alcohol (EVOH) is a formal copolymer of ethylene and vinyl alcohol. Because the latter monomer mainly exists as its tautomer acetaldehyde, the copolymer is prepared by polymerization of ethylene and vinyl acetate to give the ethylene vinyl acetate (EVA) copolymer followed by hydrolysis. EVOH copolymer is defined by the mole % ethylene content: lower ethylene content grades have higher barrier properties; higher ethylene content grades have lower temperatures for extrusion.

The plastic resin is commonly used as an oxygen barrier in food packaging. It is better than other plastics at keeping air out and flavors in, is highly transparent, weather resistant, oil and solvent resistant, flexible, moldable, recyclable, and printable [7,8]. Its drawback is that it is difficult to make and therefore more expensive than other food packaging. Instead of making an entire package out of EVOH, manufacturers keep costs down by coextruding or laminating it as a thin layer between cardboard, foil, or other plastics. Due to its strong barrier against oxygen and gas, food packaging manufacturers use EVOH in their packaging structure to extend the shelf life of food products.

Acrylonitrile is an organic compound with the formula $CH_2CHCN$ and the structure $H_2C=CH-C\equiv N$. It is a colorless, volatile liquid. It has a pungent odor of garlic or onions. Its molecular structure consists of a vinyl group ($-CH=CH_2$) linked to a nitrile ($-C\equiv N$). It is an important monomer for the manufacture of useful plastics such as polyacrylonitrile. It is reactive and toxic at low doses.Acrylonitrile is one of the components of ABS plastic. Acrylonitrile is an organic compound with the formula $CH_2CHCN$ and the structure $H_2C=CH-C\equiv N$. It is a colorless, volatile liquid although commercial samples can be yellow due to impurities. It has a pungent odor of garlic or onions [4]. Its molecular structure consists of a vinyl group ($-CH=CH_2$) linked to a nitrile ($-C\equiv N$). It is an important monomer for the manufacture of useful plastics such as polyacrylonitrile. It is reactive and toxic at low doses [9,10].

Semiconductor photocatalysis is one most new technology for remediation of microplastics with solar light energy. TiO2 and ZnO have been photocatalytically active for degradation of pollutants but they respond only to ultraviolet light, which is just 4% of the total sunlight. This urges the researchers to develop cost effective visible-light-driven photocatalyst. Photocatalytic degradation is regarded as an environmentally friendly purification method with high-efficiency. During excitation of nanoparticles, and a pair of electrons and holes are produced in the redox reaction. In this process, it is possible to degrade the (micro) plastics into smaller inorganic molecules, such as carbon dioxide and water. Many studies have demonstrated the good (micro) plastics degradation efficiency of the photocatalytic technology. However, limited information is available on the recent advances in the photocatalytic degradation of (micro) plastics. Some nano/microstructured metal oxide semiconductors were effective photocatalysts for microplastic degradation. The modifications made to nano/microstructured metal oxides such as TiO2, ZnO, bismuth oxyhalides (BiOX), NiO, Cu2O/CuO, perovskite-like Bi2WO6, Fe3O4, etc., to enhance their degradation efficiency [11,12].

Cellulose is a poly-saccharide that is chemically composed of glucose along with β-(1–4) glycosidic bond, surrounded by lignin and interrupted with hemicelluloses. The isolated cellulose is non-toxic, biodegradable and economical in comparison to other supports like graphene, and graphene oxide. Due to its narrow band-gap, high stability, effective photocatalytic activity, and non-toxicity, cellulose is a support for mineral synthesis since contais natural polymers exhibited biodegradability. It is eco-friend organic carbon and is a natural resource [10-12]. Cellulose nanocomposites was extensively used sin their low cost, high chemical durability and excellent mechanical properties [11-13]. Due to the low polymerization and large surface area cellulose is a polymeric material to generate nanocomposite materials by addition of other inorganic moeities [12]. A lot of studies was performed with bonding cellulose to Ag@AgCl and to CuS- for photodegradation of dyes. TiO2 was combining with cellulose photodegrade phenol based pollutants under UV light [10-12].

Amongst the vanadium oxides vanadium dioxide (VO2), is a semiconductor with narrow band gap energy [14]. Therefore, VO2 is used in the photooxidation to produce nanocomposite due to shape and energy saving properties [15]. However, VO2 is extensively used for dye photodegradation. Since VO2 has high redox reactions by donding of some slow the recombination of the electron–pairs non metal dopants was added to VO2. Doping of the VO2 with non-metal N, C and S, modifies the photocatalytic yields with introducing additional energy in bands. This results with trapping of electrons separate carriers from the bands in the surface of nanocomposite [6-8]. These moeities improve the transtion of charge carriers to during illumination [5-8].

To the best of our information, a nanocomposite of Cellulose/S/VO2 has not yet been investigated in the photodegradation of ethylene vinyl alcohol and acrylonitrile microplastics. Therefore, in this study the optimization of the Cellulose/S/VO2 was performed by investigating the effects of some conditions like time, pollutant concentration, nanocomposite concentration, Ph, temperature and sun light power. For maximal photodegradation efficiencies of ethylene vinyl alcohol and acrylonitrile microplastics the optimal operational and environmental matrix were determined. The physicochemical properties of the generated nanocomposite were performed with X-ray diffractometer (XRD), Fourier transform infrared (FT-IR, Raman analysis, X-ray photoelectron spectroscopy (XPS), field emission scanning electron microscope (FE-SEM) equipped with EDX and a high-resolution transmission electron microscope (HR-TEM). The reusability of the Cellulose /S/VO2 nanocomposite was performed during 90 times operation.

## MATERIALS AND METHODS

### Preparation of Cellulose

15 g of cotton fibers was put in 750 mL 3 M HCl. The mixture was stirred for 3 h. Then it was centrifuged for 10 min and rinsed with deionized water . It was dried at 80 °C for 364 h.

### Generation of S-VO2

S and VO2 was mixed at ratios of 1:1.6 for V2O5/S and 1:1,2 for Cellulose/(V2O5+S), respectively. A total of 12,45 g of cellulose was added into 60 mL of deionized water. It was stirred for 2 h, and left to stand 2 days. 8 g of S was put into 60 mL of distilled water water having 1 g diethanolamide to ensure the homogenous mixture of S. Then the mixture was mixed for 2 h. Afterwards, 6.89 g of V2O5 was put.

### Generation of Cellulose/S-VO2 nanocomposite

2 mg of cellulose was mixed to V2O5-S mixture. Then the solution was remained at 2000 ◦ C for 32 h. The obtained product was separated and washed with ethanol. It was dried under vacuum at 80 ◦ C and stored in a teflon cup.

### Measurements of ethylene vinyl alcohol and acrylonitrile microplastics

The concentrations of both microplastics were determined with gel permeation chromatography at 50 °C with Shodex SB-802.5 HQ and Shodex SB-804 HQ columns (Tokyo, Japan) and a RID-20A refractive index detector (Kyoto, Japan).

### Physicochemical analysis of Cellulose/S/VO2 nanocomposite

The structure of the nanocomposite was characterized by X-ray diffractometer (XRD), Bruker model D8 Advance, with Cu-Kα radiation . The crystalline phase of the Cellulose/S/VO2 nanocomposite was identified by comparing the major peak positions with standard JCPDS files. The main groups were characterized using Fourier transform infrared (FT-IR), Thermo Scientific, at 3980–420 $cm^{-1}$ range. Raman analysis was measured with a dispersive Raman spectrometer equipped with an microscope. The surface composition and chemical state of the nanocomposite were characterized by X-ray photoelectron spectroscopy (XPS), Thermo Fisher Scientific. The morphology of the products was examined by a field emission scanning electron microscope (FE-SEM) (Quanta 250 FEG, Field Emission Gun) equipped with EDX. A high-resolution transmission electron microscope (HR-TEM; JEM-2100),was used for elemental composition.

### Photocatalytic studies

Certain amount of microplastic samples taken from an paper industry solid wastes was

Mixed with certain amount of cellulose/S/VO2 nanocomposite in a teflon coated glass reactor under different sun ligth powers and mixed continously at certain times and pHs

The properties of ethylene vinyl alcohol and acrylonitrile microplastics

The physicochemical properties of both microplastics were given in Picture 1a and 1b.

## RESULTS AND DISCUSSION

### XRD analysis results of S and VO2 containing Cellulose

Figure 1 exhibits the XRD analysis results of Cellulose, S, S-VO2, and Celulose/S-VO2 nanocomposite. The XRD pathway of S exhibited similarities with the S8 orthorhombic S with specific lattice parameters of a = 11.097 Å, b = 13.094 Å, and c = 25.0093 Å while the XRD disturbance of celulose indicated the specific raw

**Ethylene vinyl alcohol**

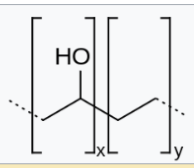


| Names | |
|---|---|
| Other names | |
| Ethenol, polymer with ethene | |
| **Identifiers** | |
| CAS Number | 25067-34-9 |
| ChemSpider | None |
| CompTox Dashboard (EPA) | DTXSID701010954 |
| **Properties** | |
| Chemical formula | $(C_2H_4O\text{-}C_2H_4)_x$ |

Except where otherwise noted, data are given for materials in their standard state (at 25 °C [77 °F], 100 kPa).

**Picture 1a:** The physicochemical properties of ethylene vinyl alcohol microplastic

**Acrylonitrile**

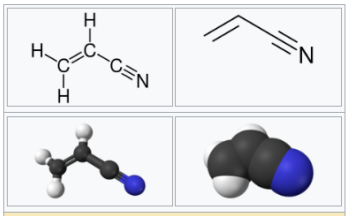


| Names | |
|---|---|
| Preferred IUPAC name | |
| Prop-2-enenitrile | |
| Other names | |
| Acrylonitrile<br>2-Propenenitrile<br>Cyanoethene<br>Vinyl cyanide (VCN)<br>Cyanoethylene[1]<br>Propenenitrile[1]<br>Vinyl nitrile | |
| **Identifiers** | |
| CAS Number | 107-13-1 ✓ |
| 3D model (JSmol) | Interactive image |
| ChEBI | CHEBI:28217 ✓ |
| ChEMBL | ChEMBL445612 ✓ |
| **Properties** | |
| Chemical formula | $C_3H_3N$ |
| Molar mass | 53.064 g·mol$^{-1}$ |
| Appearance | Colourless liquid |
| Density | 0.81 g/cm$^3$ |
| Melting point | −84 °C (−119 °F; 189 K) |
| Boiling point | 77 °C (171 °F; 350 K) |
| Solubility in water | 70 g/L |
| log *P* | 0.19[2] |
| Vapor pressure | 83 mmHg[1] |
| **Hazards** | |
| **Occupational safety and health** (OHS/OSH): | |
| Main hazards | flammable<br>reactive<br>toxic |

**Picture 1b:** Physicochemical properties of acrylonitrile microplastics

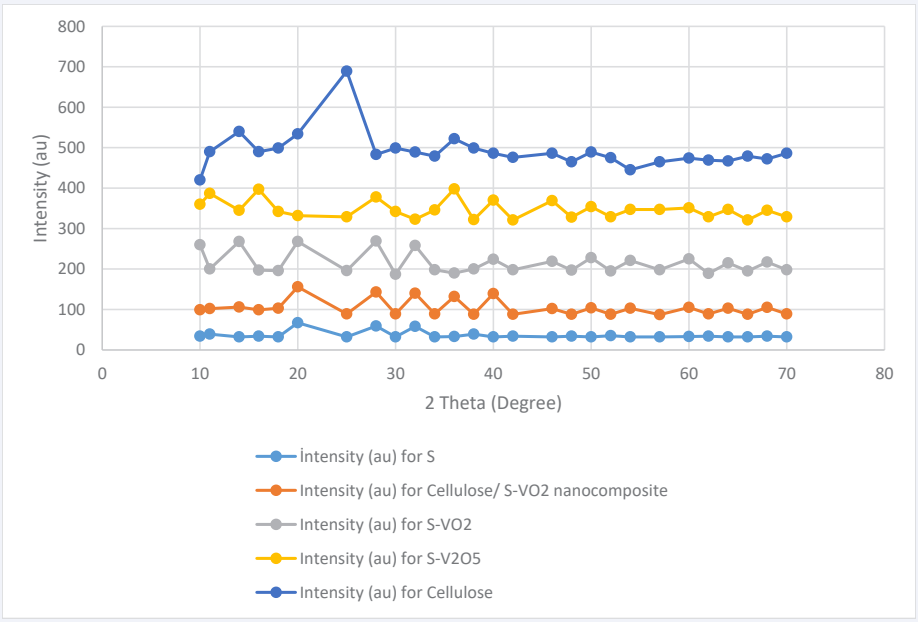


**Figure 1** XRD analysis results of Cellulose, S, S-VO2, and Celulose/S-VO2 nanocomposite

properties of cellulose (Figure 1). No other peaks was confirmed showing the presence of pure celulose . The XRD patterns of S-VO2 and cellulose/S-VO2 nanocomposite showed that V2O5 was not detected since was reduced to VO2 from V5+ to V4+ (data not shown).For S-VO2, the characteristic diffraction peaks for VO2 exhibited a monoclinicand orthorhombic structure at 2θ = 13.9◦ , 14.7◦ , 24.9◦ , 30,2◦ , 31.8◦ , 34.7◦ , 46.1◦ , 47.3◦ , and 50.3◦ with crystal disturbances of (002), (203), (102), (024), (408), (316), (004), (606), and (023), respectively. The XRD disturbances of the Cellulose/S-VO2 exhibited monoclinic crystalline properties with maximal peaks of cellulose at 2θ = 16.0◦ , 17.1◦ , and 23.2◦ . This result can the defined to the tiny dispersion of the S/ V2 surrounding of cellulose. The XRD disturbances at 2θ for 24.1◦ , 26.3◦ , 27.1◦ , and 28.3◦ was found both in S-VO2 and Cellulose/S-VO2 nanocomposite. This showed that S moieties was doped to the Cellulose/ S-VO2 nanocomposite surrounding. The diameter of sizes of the Cellulose/S-VO2 nanocomposite was calculated using the Debye–Scherrer Equation 1 .

$$D = 0.9\lambda / \beta\cos\theta_B \qquad \text{(Equation 1)}$$

where $\theta_B$, β, and λ are the Bragg diffraction angle, diffraction peak full width at half maximum (FWHM), and wavelength of the X-ray radiation (nm), respectively. The diameters of the V2O5, S-VO2, and Cellulose/S-VO2 nanocomposite was calculated as 52,09, 51.05, and 31.99 nm, respectively (data not shown) .

### FT-IR analysis results of Cellulose, S, S-VO2, and Celulose/S-VO2 nanocomposite

The FT-IR spectra for S-VO2 and Cellulose/S-VO2 nanocomposite showed a abroad band between 3230 and 3650 $cm^{-1}$ with maximal disturbancesvarying between 1534 and –1690 $cm^{-1}$(Figure 2). This can be attributed to bonding of OH groups. The disturbances at 13$cm^{-1}$ and 1119 $cm^{-1}$ exhibited the presence of S-VO2 and Cellulose/S-VO2 nanocomposite. This can be rexplained by doping of S to the VO2 surface [15-17]. The FT-IR spectroscopy of the Cellulose exhibited an unknown band at a region of 3600–3400 $cm^{-1}$ and a sligthly weak band at 1709 $cm^{-1}$.This can be attibuted to the bonding variations of OH groups. The bands present at 2990 and 1398 $cm^{-1}$ is relevant to C-H moeities. The band around 1396 $cm^{-1}$ can be attributed to C-H bound deformations. The band at 1174 $cm^{-1}$ can be defined with C-O-C ring. The band at 903 cm−1 was correlated to the β-glycosidic moeities disturbances between the glucose in cellulose]. The FT-IR spectrum of V2O5 showed three bonding bands at 1029, 897, and around 498 $cm^{-1}$. The FT-IR spectra for S-VO2 and Cellulose/S-VO2 nanocomposite showen an unknown band around 3400–3700 $cm^{-1}$. Furthermore, a maximal band around 1490–1705 $cm^{-1}$, was found. This can be attributed to OH groups. The bands at 1145 $cm^{-1}$ and 1029 $cm^{-1}$ for S-VO2 and Cellulose/S-VO2 nanocomposite can be explained by the doping of sulfur to the VO2 surface. The bands at 1030 and 1056 $cm^{-1}$ for MCC/S-VO2 and S-VO2, respectively, are attributed to O=V=O vibration. The initial disturbances band at 617 cm−1 for S-VO2 and 529 $cm^{-1}$ for Cellulose/S-VO2 can be defined with the V–O–V bending structures of VO2. The band at 719 cm−1 for Cellulose/S-VO2 was attributed to vibration of V=O . The absence of V2O5 illustrated the formation of VO2. The disturbances at 2909, 1438, 1376, 1063, 1169, and 899 cm−1 shows the bonds between S-VO2 and Cellulose [16-18]. The bands between 2911 and 1442 cm−1 shows to C-H stretching. The band at 17 cm−1 is attributed to the deformations in C-H bands. The band at 14 cm−1 is relevant the C-O-C pyranose. Furthermore, the band

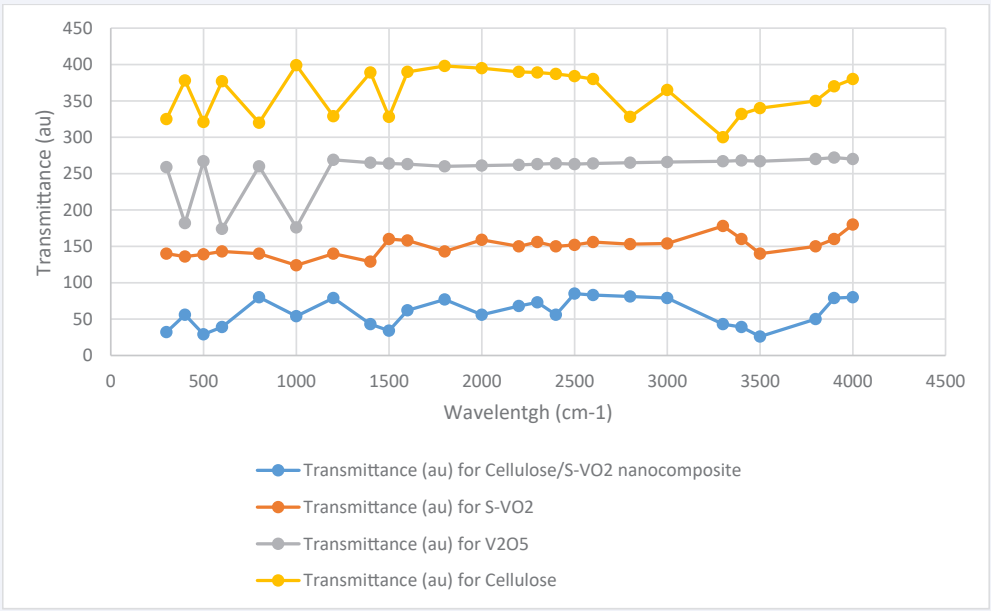


**Figure 2** FT-IR analysis of FT-IR analysis results of Cellulose, S, S-VO2, and Celulose/S-VO2 nanocomposite

at 899 cm−1 is β-glycosidic vibration. V2O5 showed maximum disturbance around 595–489 cm−1 indicating the orthorhombic V2 [19,20].

### Raman spektroscopy of Cellulose, S, S-VO2, and Celulose/S-VO2 nanocomposite

Raman spectroscopy is a very robust tool distinguishing the different crystalliphases and the change in the surface structure. The Raman spectrum of MCC/S-VO2presented in Figure 3. The Raman scattering peaks appeared at 1200, 1312, and 1520 $cm^{-1}$. The symmetry modes of the prepared sample belong to Ag and respectively. The peaks between 82 and 471 $cm^{-1}$ are assigned to the sulfur S8 orthorhobic system [21-23]. The peaks at 1419 and 1520 $cm^{-1}$ are assigned to the microcrystalline clulose [24]. There are noother peaks which can be observed.

## XPS analysis results of FT-IR analysis results of Cellulose, S, S-VO2, and Celulose/S-VO2 nanocomposite

Figure 4 shows the XPS survey for the Cellulose/S-VO2 nanocomposite. This figure shows the existance of C, O, S, and V. The C 1s disturbances for Cellulose/S-VO2 nanocomposite exhibits the presence of C, O, S, and V elements (Figure 4a). Figure 4b indicates, the C 1s which is the maximal disturbance broken down in the Cellulose/S-VO2 nanocomposite. The first maximal disturbance peak was shown at 279.09 eV. This indicates the C–C bonds, while the second maximal disturbance peak was detected at 289.98 eV. This could be attributed C–OH groups. The peak at 293.9 eV indicates the C–O bond rings [25-28]. Figure 4c indicates two maximal disturbances at 534.7and 541.2 eV which can be attributed to O bound. The peak at 533.4 eV indicates to the lattice O for VO2 [29]. The maximal disturbance at 529.2 eV can be explained by C–OH and C–O–C bound in Cellulose [30]. The S 2p XPS peaks in Figure 4d, showed an alone broad disturbance as S 2p3/2 at 163.8 eV. This can be explained by the S doping to generate of a V–S bond. By taken into consideration the vanadium sulfides, S was bonded to V and exhibited high disturbances atr S 2p peak between 162.9 and 165.8 eV [67]. The Xspectrum of V 2p (data not shown). The peaks at 528.5 and 528.8 eV can be attributed to 2p3/2 bounding energies of V5+ and V4+, respectively.

## Effects of initial ethylene vinyl alcohol and acrylonitrile microplastics concentration on the photoremovals of ethylene vinyl alcohol and acrylonitrile

In order to study the effect of initial microplastic concentration on the photocatalytic activity their removals the both microplastic concentrations increased from 50 mg/l up to 900 mg/l at a constant Cellulose /S/VO2 nanocomposite concentration of 1.8 mg/l based on data obtained from preliminary studies (data not shown. The photodegradation efficiencies of vinyl alcohol and acrylonitrile microplastics increased as the microplastic concentration increased from 50 mg/l up to 700 mg/l. The maximum vinyl alcohol and acrylonitrile microplastic yields were recorded as 98% and 96% after 40 min photodegradation time, respectively (Table 1). This situation can be explained by the formation of OH% radical on the surface of Cellulose /S/WO2 nanocomposite and the reaction of microplastics with the OH% radicals. The initial increase in the photodegradation efficiencies with increase in initial microplastic concentrations reaction between the microplastic molecules and OH% radical ending with activation of nanocomposite and continuous redox reactions between conduction band and valence band. Furher increase of microplastic concentrations to 750 and 800 mg/l did

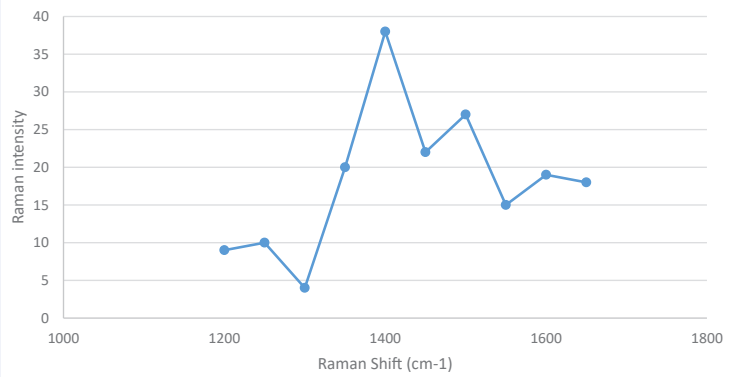


**Figure 3** Raman Spectroscopy results of Cellulose, S, S-VO2, and Celulose/S-VO2 nanocomposite

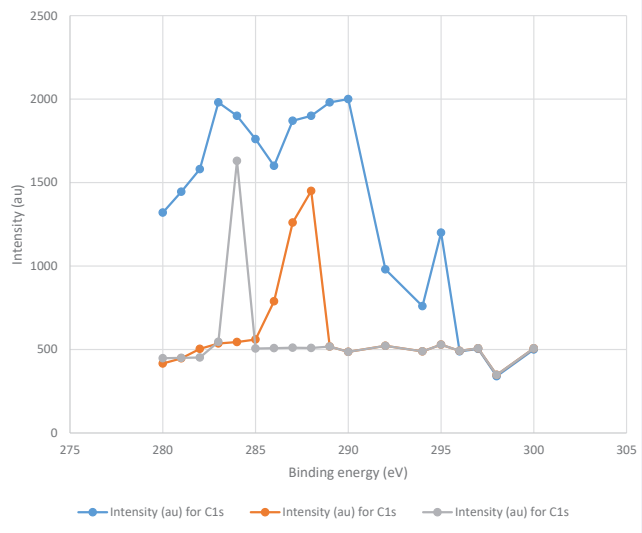


**Figure 4a** XPS analysis results of C1s in Cellulose/S-VO2 nanocomposite

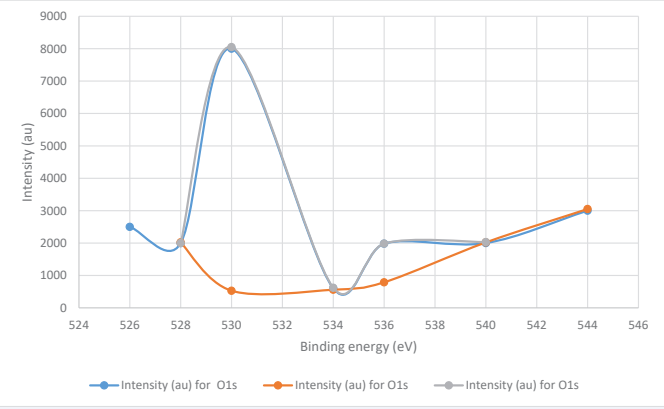


**Figure 4b** XPS analysis results of the C 1s during maximal disturbance in the Cellulose/S-VO2 nanocomposite

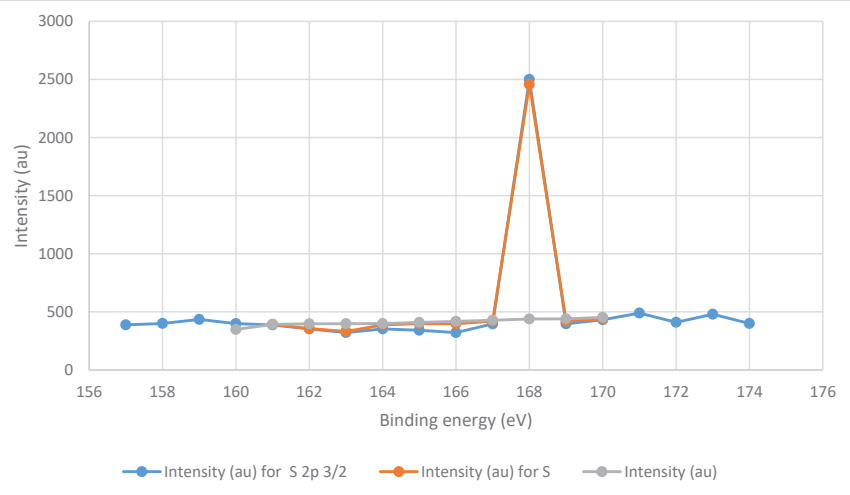


**Figure 4c** XPS analysis of maximal disturbances indicating the O bound in the Cellulose/S-VO2 nanocomposite

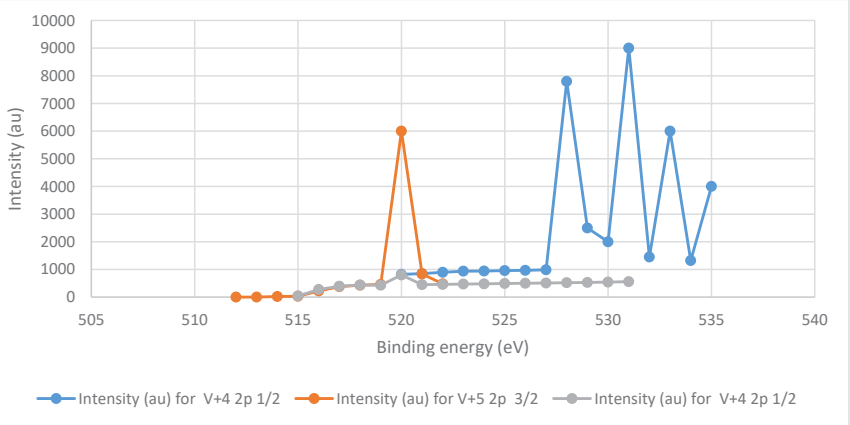


**Figure 4d** Doping to V–S bond in the Cellulose/S-VO2 nanocomposite in the Cellulose/S-VO2 nanocomposite

**Table 1:** Effects of initial ethylene vinyl alcohol and acrylonitrile microplastic concentrationS on the photodegradation of ethylene vinyl alcohol and acrylonitrile

| Initial ethylene vinyl alcohol and acrylonitrile microplastics concentration (mg/l) | vinyl alcohol photodegradation yield (%) | acrylonitrile photodegradation yield (%) |
|---|---|---|
| 50 | 98 | 96 |
| 100 | 98 | 96 |
| 150 | 98 | 96 |
| 200 | 98 | 96 |
| 250 | 98 | 96 |
| 300 | 98 | 96 |
| 400 | 98 | 96 |
| 500 | 98 | 96 |
| 600 | 98 | 96 |
| 650 | 98 | 96 |
| 700 | 98 | 96 |
| 800 | 88 | 80 |
| 900 | 80 | 75 |

not affect the yields and photodegradation efficiencies of both microplastics (31-34). This can be explained by the inhibition process of the redox reactions between the nanocomposite molecules and OH% radicals. High microplastic concentrations adsorbed on the surface of Cellulose /S/WO2 nanocomposite this ending with reduced nanocomposite activation and OH productions. In other words inhibited number of activities accessible on the surface of the nanocomposite.A competition between active reaction sites and photons on the surface of nanocomposite was occurred. At high microplastic concentration the pollutant will occupy a greater number of nanocomposite preventing the oxidation of pollutants and their metabolites and ending with slowing breakdown rates. Furthermore, high microplastic concentration necessitates greater amount of photon absorption. Lesser photons available to activate the nanocomposite, resulting in decreased photocatalytic activity in the inactivated nanocomposite surface (35-37).

## Effect of pH on ethylene vinyl alcohol and acrylonitrile microplastics photoremovals

The pH of a solution is an important operating parameter affecting the photocatalytic activity of the Cellulose /S/WO2 nanocomposite since Ph affect significantly charge properties of the Cellulose /S/WO2 nanocomposite surface. The pH of the microplastic mixtures was adjusted to 4, 7 and 10 (Table 2). The Photodegradation percentage of both microplastics increases with the increase in pH from 4 to 10. Under acidic pH conditions, the photodegradation efficiency is low since the dissolution of VO2. The zero point charge of VO2 is at pH-8. Above this pH value, Cellulose /S/WO2 nanocomposite surface is negatively charged while both microplastics have positive charge. Due to electrostatic interaction between the negatively charged nanocomposite surface and positively charged microplastics high photodegradation yields was detected under alkaline conditions compared to acidic Ph conditions (38,39). For maximum vinyl alcohol (99%) and acrylonitrile (97%) microplastic photodegradation yields the optimal pH values should be 10. At lower pH, the photodegradation yields decreased due to the low hydroxyl group. This limited the photodegradation efficiency and reduced the production of free radicals on the surface of nanocomposite under sun light irradiation (40-42).

## Efect of time on the photodegradation yields of ethylene vinyl alcohol and acrylonitrile microplastics

The degradation of microplastics was significantly affected by photodegradation time. For example, the micropllutant breakdown yields via photodegradation increased from around 38-40% to 97-99% afte 35 min (Table 3). As it would be expected, the photodegradation efficiency of microplastics elevated with an increased exposure time (43).

## Effect of Cellulose/S/WO2 nanocomposite concentrations on the photodegradation yields of ethylene vinyl alcohol and acrylonitrile microplastics

The Cellulose/S/WO2 nanocomposite concentration affects significantly the performance of a photocatalytic process. For economical point of view the least amount of nanocomposite should be taken into consideration for maximal microplastic photodegradation yields. When the nanocomposite concentrations is low (0,5 and 1 mg/l) the generation of reactive species like OH, H202 and O decreased on the surface of the Cellulose /S/WO2 nanocomposite This cause to lowered of photocatalytic reactions. The maximum photodegradation yields for vinyl alcohol and acrylonitrile microplastics was found to be 1.9 mg/l (Table 4). A significant statistical correlation between the

**Table 2:** Effect of increasing pH on ethylene vinyl alcohol and acrylonitrile microplastic photodegradation yields

| Ph | vinyl alcohol photodegradation yield (%) | acrylonitrile photodegradation yield (%) |
|---|---|---|
| 4 | 45 | 40 |
| 7 | 57 | 50 |
| 10 | 99 | 97 |

**Table 3:** Efect of photodegradation time on the photodegradation yields of ethylene vinyl alcohol and acrylonitrile microplastics

| Photodegradation time (min) | vinyl alcohol photodegradation yield (%) | acrylonitrile photodegradation yield (%) |
|---|---|---|
| 5 | 40 | 38 |
| 10 | 50 | 45 |
| 15 | 70 | 66 |
| 20 | 75 | 70 |
| 25 | 80 | 74 |
| 30 | 90 | 84 |
| 35 | 99 | 97 |
| 40 | 98 | 96 |
| 45 | 98 | 96 |
| 50 | 98 | 96 |
| 55 | 98 | 96 |
| 60 | 88 | 80 |
| 70 | 80 | 75 |

**Table 4:** Effect of Cellulose /S/WO2 nanocomposite doses on the photodegradation yields of ethylene vinyl alcohol and acrylonitrile microplastics

| Cellulose /S/WO2 nanocomposite concentrations (mg/l) | vinyl alcohol photodegradation yield (%) | acrylonitrile photodegradation yield (%) |
|---|---|---|
| 0,5 | 63 | 60 |
| 1.0 | 80 | 76 |
| 1.5 | 90 | 84 |
| 1.9 | 99 | 97 |
| 2.5 | 95 | 90 |
| 3 | 90 | 88 |
| 3.4 | 88 | 82 |
| 4 | 80 | 79 |
| 5 | 70 | 60 |
| 6 | 60 | 50 |

photodegradation efficiency and nanocomposite concentration was found up to an optimal nanocomposite concentration is attained. At high nanocomposite concentrations can result in turbidity and a blocking effects of active points on the surface of nanocomposite. This cause to decreasing light intensity in the nanocomposite microplastic matrix. Decreased sunlight transmission with elevated nanocomposite concentration cause to lowered of photodegradation of microplastics (8-12). On the other hand, at optimal nanocomposite doses, the nanocomposite has good agglomeration due to its high surface energy. Therfore the optimal nanocomposite concentrations excellent photocatalytic yields was detected.

## Effect of sun ligth intensity on the photodegradation yields of ethylene vinyl alcohol and acrylonitrile microplastics

During sun light irradiation, photon/ quantum yields affect significantly the photocatalytic degradation process. In this study the sun ligth intencity was increased from 30 W/m2 up to 90 W/m2. The maximal ethylene vinyl alcohol and acrylonitrile microplastics photodegradation yields was detected at a sun ligth power of 60 W/m2 as 99% and 97%, respectively (Table 5). The photodegradation yields of these microplastics increased from 78% and 79% up to maximum yields as the sun ligth power was increased from 30 W/m2 up to 60 W/m2. Light irradiation generates energy required for electron activation from the

**Table 5:** Effect of sun ligth intensity on the photodegradation yields of ethylene vinyl alcohol and acrylonitrile microplastics

| Sun ligth intensity (W/m2 | vinyl alcohol photodegradation yield (%) | acrylonitrile photodegradation yield (%) |
|---|---|---|
| 30 | 78 | 79 |
| 40 | 83 | 81 |
| 50 | 90 | 88 |
| 60 | 99 | 97 |
| 70 | 98 | 95 |
| 80 | 96 | 90 |
| 90 | 96 | 89 |

**Table 6:** Effect of temperature on the photodegradation yields of ethylene vinyl alcohol and acrylonitrile microplastics

| Temperature (°C) | vinyl alcohol photodegradation yield (%) | acrylonitrile photodegradation yield (%) |
|---|---|---|
| 10 | 79 | 76 |
| 20 | 80 | 81 |
| 30 | 83 | 82 |
| 40 | 90 | 90 |
| 50 | 99 | 97 |
| 60 | 96 | 90 |
| 90 | 96 | 89 |

**Table 7:** Rreuse of Cellulose /S/VO2 nanocomposite

| Run | vinyl alcohol photodegradation yield (%) | acrylonitrile photodegradation yield (%) |
|---|---|---|
| 1 | 99 | 97 |
| 2 | 99 | 97 |
| 3 | 99 | 97 |
| 4 | 99 | 97 |
| 5 | 99 | 97 |
| 6 | 99 | 97 |
| 7 | 99 | 97 |
| 8 | 99 | 97 |
| ..... | 99 | 97 |
| 20 | 99 | 97 |
| 21 | 99 | 97 |
| 22 | 99 | 97 |
| .... | 99 | 97 |
| 30 | 98 | 96 |
| 31 | 98 | 96 |
| 32 | 98 | 96 |
| 33 | 98 | 96 |
| ..... | 98 | 96 |
| 40 | 98 | 96 |
| 41 | 98 | 96 |
| 42 | 98 | 96 |
| ..... | 98 | 96 |
| 50 | 98 | 96 |
| 51 | 98 | 96 |
| 52 | 98 | 96 |
| ..... | 98 | 96 |
| 60 | 97 | 95 |
| 61 | 97 | 95 |
| 62 | 97 | 95 |
| .... | 97 | 95 |
| 70 | 97 | 95 |
| 71 | 97 | 95 |
| 72 | 97 | 95 |
| .... | 97 | 95 |
| 80 | 97 | 95 |
| 81 | 97 | 95 |
| .... | 97 | 95 |
| 90 | 96 | 94 |
| 91 | 96 | 94 |

valence band to the conduction band of the nanocomposite (43). Since the power of the light indicates the whole energy reguired for a photodegradation metrix, and each photon affected bt the ligth wavelength, ligth intensity is significantly important. The dependence of the wavelength on photodegradation is also related to the absorption/photodegradation spectrum of the irradiated microplastics. For photons to be absorbed, the spectrum of the irradiation source should overlap with the absorption spectrum of the nanocomposite. Due to their excellent bandgap (Eg > 3.0 eV) of Cellulose /S/WO2 nanocomposite at sun ligth power of 60 W/m2 exhibited perfect photodegradation yields.

### Effect of temperature on the photodegradation yields of ethylene vinyl alcohol and acrylonitrile microplastics

In order to detect the effects of temperature on the photodegradation yields of both microplastics the temperature was increased from 10°C up to 60°C. The maximal photodegradation yields was detected at 50°C (Table 6). Further increase of temperature did not affect the yields of micropollutants. Elevated temperatures affect positively the charge carrier under nanocomposite for recombination of redox reactions cause increasing of photodegradation yields (8-11). Photodegradation yields was high at 50°C. An optimal range for temperature is necessary for photodegradation of microplastics. This value was found to be 50°C.

### Reusability of Cellulose /S/VO2 nanocomposite

To study the reusability of the Cellulose /S/WO3 nanocomposite 90 times the same nanocomposite was used. After 30 time utilisation, the photodegradation yields of ethylene vinyl alcohol and acrylonitrile microplastics reduced sligtly to 98% and 96% (Table 7). After 60 time utilization the yields decreased to 97% and 95% while after 90 time usage the yields was decreased only to 96% and 94% for both microplastics, respectively. The reusability of nanocomposites are important considerations when choosing a cost-effective nanocomposite for large-scale photodegradation assays.

## CONCLUSIONS

Cellulose/S/VO2 nanocomposite is a promising nanocatalyst with high photodegradation capacity to degrade the vinyl alcohol and acrylonitrile microplastics with yields as high as 99% and 97% with an economic dosage as low as 1.9 mg/l.To investigate the stability of cellulose/S/VO2 nanocomposite XRD, XPS, Raman and FT-IR characterizations were performed and for maximal vinyl alcohol and acrylonitrile microplastic photodegradation efficiencie,s the optimal operational and environmental conditions were identified. The orthorhombic structure of S and monoclinic crystal shape of VO2, doping of S to VO2 surface, C–OH and C–O–C bounds in cellulose and OH attachements in the Cellulose/S/VO2 nanocomposite exhibited excellent photodegradation yields to degrade both microplastics. The Cellulose/S/VO2 nanocomposite had excellent reusability

and remarkable selectivity to remove the vinyl alcohol and acrylonitrile microplastics. After 90 time utilization of the same nanocomposite the micropollutant yields decreased only to 96% and 94%.

## REFERENCES

1. Yang L, Zhang Y, Kang S, Wang Z, Wu C. Microplastics in soil: a review on methods, occurrence, sources, and potential risk, Sci. Total Environ. 2021; 780: 146546
2. Eriksen M. Plastic pollution in the World's oceans: more than 5 Trillion plastic pieces weighing over 250,000 tons Afloat at sea, PLoS One. 2014; 9: 1-15.
3. Gasperi J. Microplastics in air: are we breathing it in? Curr Opin Environ Sci Heal. 2018; 1: 15.
4. Zhao T, Lozano YM, Rillig MC. Microplastics increase soil pH and decrease microbial activities as a function of microplastic shape, polymer type, and exposure time. Front Environ Sci. 2022; 9: 1–14.
5. Mani T, Hauk A, Walter U, Burkhardt-Holm P. Microplastics profile along the Rhine river. Sci Rep. 2015; 5: 1-7.
6. Osorio ED, Tanchuling MAN, Diola MBLD. Microplastics occurrence in surface waters and sediments in five river Mouths of Manila Bay. Front Environ Sci. 2021; 9: 1-14.
7. Schernewski G, Radtke H, Hauk R, Baresel C, Olshammar M, Oberbeckmann S. Urban microplastics Emissions: Effectiveness of retention Measures and consequences for the Baltic sea, Front Mar Sci. 2021; 8.
8. Chia WY, Ying Tang DY, Khoo KS, Kay Lup AN, Chew KW. Nature's fight against plastic pollution: algae for plastic biodegradation and bioplastics production. Environ Sci Ecotechnology. 2020; 4: 100065.
9. Wu C, Zhang K, Xiong X. Microplastic pollution in inland waters focusing on asia, in: M. Wagner, S. Lambert (Eds.), Freshwater Microplastics. Emerging Environmental Contaminants?, Springer. 2018; 85-99.
10. Westphalen H, Abdelrasoul A. Challenges and treatment of microplastics in water, in: M. Glavan (Ed.), Water Challenges of an Urbanizing World, intechopen, 2018.
11. Dey TK, Uddin ME, Jamal M. Detection and removal of microplastics in wastewater: evolution and impact. Environ Sci Pollut Res. 2021; 28: 16925-16947
12. Malankowska M, Echaide-Gorriz C, Coronas J. Microplastics in marine environment: a review on sources, classification, and potential remediation by membrane technology. Environ Sci. 2020; 20: 1678-1689.
13. Bui XT, Vo TDH, Nguyen PT, Nguyen VT, Dao TS, Nguyen PD. Microplastics pollution in wastewater: characteristics, occurrence and removal technologies. Environ Technol Innov. 2020; 19: 101013
14. Franco AA, Arellano JM, Albendín G, Rodríguez-Barroso R, Quiroga JM, Coello MD. Microplastic pollution in wastewater treatment plants in the city of C´ adiz: abundance, removal efficiency and presence in receiving water body. Sci Total Environ. 2021; 776: 145795
15. Schwabl P. Detection of various microplastics in human stool: a prospective case series. Ann Intern Med. 2019; 171: 453-457
16. Ragusa A. Plasticenta: first evidence of microplastics in human placenta. Environ Int. 2021; 146: 106274.
17. Ragusa A, Svelato A, Belloni A, Gioachhani G, Blondeel C, Zucchelli E, et al., Raman microspectroscopy detection and characterisation of microplastics in human breastmilk, Polymers. 2022; 14: 1–14.
18. Tursi A, Baratta M, Eston T, Chatzisymeon E, Chidichimo F, De Baise M, et al. Microplastics in aquatic systems, a comprehensive review: origination, accumulation, impact and removal technologies, RSC Adv. 2022; 12: 28318-28340
19. Schymanski D, Goldbeck C, Humpf HU, Fürst P. Analysis of microplastics in water by micro-Raman spectroscopy: release of plastic particles from different packaging into mineral water, Water Res. 2018; 129: 154-162.
20. Cox KD, Covernton GA, Davies HL, Dower JF, Juanes F, Dudas SE. Erratum: human consumption of microplastics. Environ Sci Technol. 2019; 53: 7068-7074.
21. Fournier E, Leveque M, Ruiz P, Ratel J, Durif C, Chalancon S, et al. Microplastics: what happens in the human digestive tract? First Water Res Technol. 2021; 7: 243-258.
22. Cox KD, Covernton GA, Davies HL, Dower JF, Juanes F, Dudas SE. Human consumption of microplastics, Environ Sci Technol. 2019; 53: 7068-7074.
23. Prata JC. Airborne microplastics: consequences to human health?, in: Environ Pollut. 2018; 234: 115-126.
24. Mason SA, Welch VG. Neratko, Synthetic polymer contamination in bottled water. Front Chem. 2018; 6: 407
25. Woo JH. Polypropylene nanoplastic exposure leads to lung inflammation through p38-mediated NF-κB pathway due to mitochondrial damage. Part Fibre Toxicol. 2023; 20: 1-17.
26. Lu W. New evidence of microplastics in the lower respiratory tract: inhalation through smoking. Environ Sci Technol. 2023; 57: 8496-8505.
27. Jenner LC, Rotchell JM, Bennett RT, Cowen M, Tentzeris V, Sadofsky LR. Detection of microplastics in human lung tissue using μFTIR spectroscopy. Sci Total Environ. 2022; 831: 154907.
28. Song S. Inhalable textile microplastic fibers impair airway epithelial differentiation. Am J Respir Crit Care Med. 2023; 69.
29. Contino M. In vitro nano-polystyrene toxicity: metabolic dysfunctions and cytoprotective responses of human spermatozoa. Biol. 2023; 12: 624.
30. Ajeya KV, Sadhasivam T, Kurkuri MD, Kang UI, Park IS, Park WS, et al. Recovery of spent VOSO4 using an organic ligand for vanadium redox flow battery applications. J Hazard Mater. 2020; 399: 123047.
31. Zhang Q, Lu Y. Change in crystallization mechanism of Sb film by doping VO2 for ultra-retention and high-speed phase change memory. Cryst Growth Des. 2019; 19: 3477-3483.
32. Meenu PK, Dehiya BS. One step hydrothermal synthesis of nanostructured VO2 (B) for photocatalytic application.. J Nanosci Technol. 2019; 5: 584-586.
33. Solis-Casados DA, Escobar-Alarcon L, Infantes-Molina A, Klimova T, Serrato-García L, Rodríguez-Castellón E, et al. Synthesis and characterization of Ag-modified V2O5 photocatalytic materials. J Chem. 2017; 5849103.
34. Gurulakshmi M, Selvaraj M, Selvamani A, Vijayan P, Rekha NS, Shanthi K. Enhanced visible-light photocatalytic activity of V2O5/S-TiO2 nanocomposites. Appl Catal A Gen. 2012; 449: 31-46.
35. Kerli S, Alver Ü, Eskalen H, Uru s, S, So ˘guksu AK. Structural and Morphological Properties of Boron Doped V2O5 Thin Films: Highly Efficient Photocatalytic Degradation of Methyl Blue. Russ J Appl Chem. 2019; 92: 304-309.
36. Vorontsov AV, Valdés H. Insights into the visible light photocatalytic activity of S-doped hydrated TiO2. Int J Hydrogen Energy. 2019; 44: 17963-17973.

37. Saleh KA, Sadiq YK. Synthesis and characterization of chrome (VI) ion/iron oxide/chitosan composite for oxidation of methylene blue by photo-fenton reaction. Chem Methodol. 2023; 7: 112-122.

38. Kalam A, Al-Sehemi AG, Assiri M, Du G, Ahmad T, Ahmad I, et al. Modified solvothermal synthesis of cobalt ferrite (CoFe2O4 ) magnetic nanoparticles photocatalysts for degradation of methylene blue with H2O2/visible light. Results Phys. 2018; 8: 1046-1053.

39. Maleki B, Sandaroos R, Naderi S, Peiman S. A crowned manganese-based Schiff complex supported on nanocellulose as an efficient and sustainable heterogeneous catalyst for the oxidation of benzyl alcohols. J Organomet Chem. 2023; 990.

40. Mohamad Haafiz MK, Eichhorn SJ, Hassan A, Jawaid M. Isolation and characterization of microcrystalline cellulose from oil palm biomass residue. Carbohydr Polym. 2013; 93: 628-634.

41. Tang AM, Hu TT, Su X. Fabrication of Microcrystalline Cellulose/CdS Nanocomposites and their Photocatalytic Properties. Adv Mater Res. 2013; 634: 2475-2480.

42. Wang Y, Zhang Z. Synthesis and field emission property of VO2 nanorods with a body-centered-cubic structure. Phys. E Low-Dimens. Syst. Nanostructures. 2009; 41: 548-551.

43. Wang Y, Zhang Z, Zhu Y, Li Z, Vajtai R, Ci L, et al. Nanostructured VO2 Photocatalysts for Hydrogen Production. ACS Nano. 2008; 2: 1492-1496.